ACS Photonics

pubs.acs.org/journal/apchd5

Article

Ultrafast Diffraction Shaping by Periodic Arrays of GaAs Nanoantennas

Dmitry N. Gulkin, Alexander S. Shorokhov, Viacheslav S. Snigirev, Sarkis A. Dagesyan, Evgeny A. Kelm, Vladimir O. Bessonov, and Andrey A. Fedyanin*

Cite This: *ACS Photonics* 2025, 12, 6254–6261

Read Online

ACCESS | Metrics & More | Article Recommendations | Supporting Information

ABSTRACT: Efficient ultrafast control of the intensity and wavefront of light is essential for many modern optical devices, from LiDAR scanning systems to advanced laser beam shapers. A CMOS-compatible approach to spatial light control is based on tailoring the directional scattering from metasurfaces made of arrays of Mie-resonant semiconductor nanoparticles—meta-atoms. All-optical ultrafast tuning is possible by generating photoinduced carriers in semiconductor meta-atoms and is usually traced by overall transient reflection or transmission. However, the high intensities of light pulses required for effective modulation impose a limit for applications. Here, we introduce a diffractive metasurface based on gallium arsenide and demonstrate that ultrafast tuning of intensity is an order of magnitude stronger for the diffracted beam than for the transmitted one. Experimentally, the intensity modulation of the first diffraction order reaches 16% at a pump fluence level of only a few $\mu J/cm^2$, with a switching time of 200 fs and a relaxation time of 1.2 ps. The results constitute an important milestone in ultrafast optical switching device development for efficient low-power spatial light control.

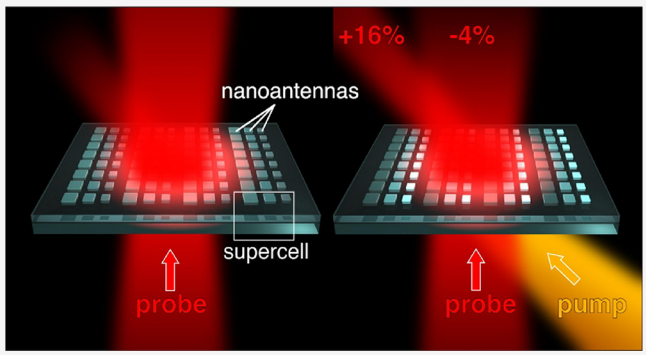

KEYWORDS: *semiconductor metasurfaces, Mie resonances, free-carriers injection, ultrafast diffraction control, pump−probe method, back focal plane microscopy*

INTRODUCTION

All-optical devices have recently gained the attention of the nanophotonics community due to the ultrafast time scale of the associated processes.[1−3] Applications based on ultrafast all-optical switching range from high-speed light modulation[4,5] and LiDAR systems[6] to neuromorphic devices.[7] Numerous light control methods use optical resonances, such as Mie-type resonances in subwavelength objects or nanoantennas.[8−11] Specifically, nanoantennas exhibiting Mie-type resonant features in scattering spectra are very common.[12] By modifying the particle shape, one can passively control the direction and propagation of light.[13−15] These morphology-dependent resonances make it possible to manipulate light below the free-space diffraction limit and get a pronounced optical magnetic response in structures with high-Q and low losses within the visible and near-infrared spectral regions.[16,17] The possibilities of optical manipulation can be extended by placing resonant nanoparticles in two-dimensional lattices, i.e., by forming metasurfaces.[18] Flexible control of reflected,[19] transmitted,[20−22] and diffracted[23] beams, including their wavelength[24] and polarization[25] handling as well as beam shaping[26] by metasurfaces has been demonstrated. Metasurfaces applicable for optical control are used in spectrometers,[27,28] holography,[29] and wavelength division multiplexing.[30]

The properties of light can be modified and controlled in an active manner, usually employing clusters of nanoparticles and metasurfaces. In this case, the amplitude, phase, and direction of light are modified using phase-change[31] or liquid-crystal media,[32] thermal[33,34] or electrical tuning,[35,36] all-optical control,[37−40] and other techniques.[41,42] In particular, the all-optical control method can alter the light parameters in the fastest way through the photogeneration of free carriers inside semiconductor nanoparticles forming a metasurface.[43,44] As a result of the subsequent ultrafast change in the refractive index of the particle material, the spectral positions of the optical resonances are shifted, which in turn modifies the reflectance and transmittance of the metasurface along with the light scattering diagram of nanoparticles at specific wavelengths.[37,38] In this context, metasurfaces based on nonmetallic materials with a high refractive index have been considered and extensively studied.[45] Particular research has focused on

Received: July 22, 2025
Revised: October 14, 2025
Accepted: October 15, 2025
Published: October 23, 2025

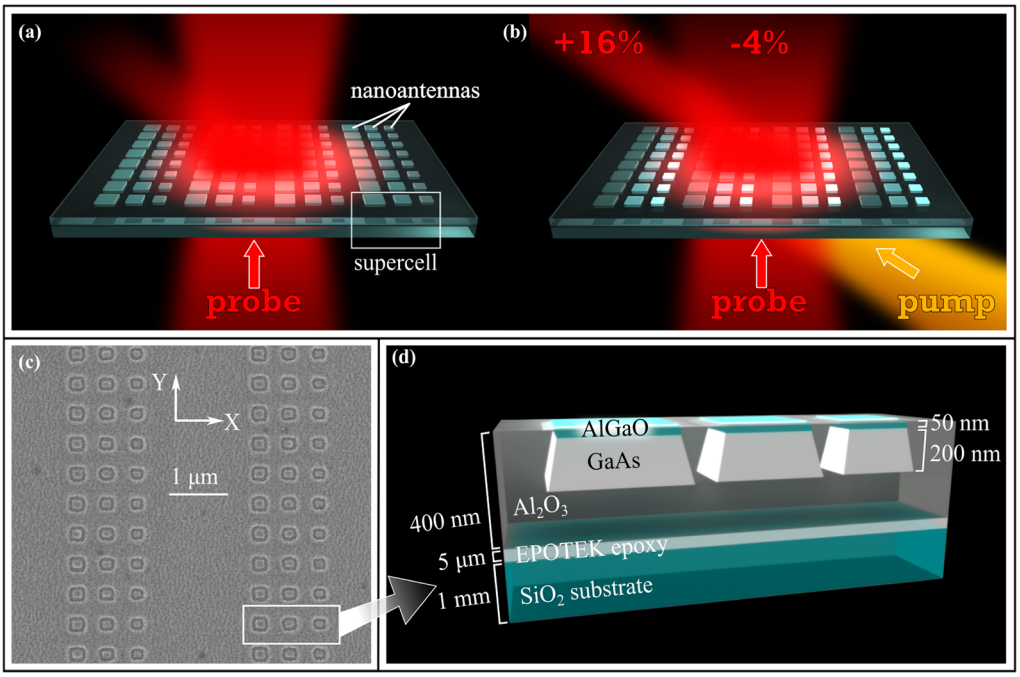

Figure 1. Semiconductor metasurface for ultrafast diffraction shaping. (a, b) Asymmetric diffraction of transmitted light before (a) and after (b) pumping. The pump-induced free-carrier generation changes the optical constants of the metasurface material, resulting in a transient redistribution of light between diffraction orders. (c) Scanning electron microscopy image of the experimental sample. The white frame highlights a supercell consisting of three gallium arsenide particles of different sizes arranged along the *X*-direction. (d) Sketch of the supercell. The structure consists of three truncated square GaAs pyramids covered by a thin AlGaO layer, embedded in an Al_2O_3 layer. The metasurface is attached to a SiO_2 substrate using a transparent epoxy.

devices based on III−V direct-gap semiconductors, such as GaAs, where an efficient free-carrier generation occurs due to direct optical transitions.[46−48]

All-optical ultrafast effects in metasurfaces are usually traced by transient changes in reflectance[49] or transmittance,[50] enhanced by the modification of the spectral line shape of optical resonances. In many cases, for a practically applicable signal modulation amplitude, the typical power densities (fluences) of the switching radiation are tens to hundreds of $\mu J/cm^2$.[51,52] The important goal of designing energy-efficient all-optical devices is therefore to reduce the pump radiation fluence without causing dramatic losses in switching performance.[48,53] One way is to harness the directional light scattering by Mie-resonant nanoparticles, which is known to be used to control the intensity of diffraction orders of a metasurface.[21,52]

In this paper, a new approach for subpicosecond low-energy optical switching is introduced that involves ultrafast modulation of the scattering diagram of meta-atoms constituting a metasurface to control the intensity of its diffraction orders. The transmission metasurface consists of periodically arranged clusters of closely placed Mie-resonant GaAs nanoantennas and acts as a diffraction grating that dynamically redistributes light between diffraction orders under optical pumping. A relaxation time of 1.2 ps and an optically induced intensity modulation of diffraction maxima of 12−17% at a low pump fluence of 4 $\mu J/cm^2$ are measured using time-resolved Fourier plane imaging microscopy.

RESULTS AND DISCUSSION

Concept. A conceptual illustration of the ultrafast all-optical control of metasurface resonant scattering is given in Figure 1. The metasurface consists of a periodic stack of supercells, each of them containing several closely packed semiconductor crystalline gallium arsenide (GaAs) particles of different sizes, which act as nanoantennas supporting Mie-type resonances. In the *X*-direction, the period of the supercell stack is large enough to observe several diffraction orders at a given wavelength. GaAs particles are designed in a way that the supercell forms a gradient phase profile of the scattered light wave, increasing the intensity of light deflected into the selected diffraction order. Figure 1a shows that the intensity of light diffraction orders to the left (orders with the numbers $m < 0$) is higher than that of diffraction orders to the right (orders with the numbers $m > 0$). At the same time, in the spectral region of the pump light, each particle of the supercell maintains a magnetic dipole (MD) resonance, the wavelength of which red-shifts as the particle size increases. When the metasurface is irradiated with pump light, the particles with different sizes absorb different amounts of pump energy, depending on the detuning between the frequencies of the pump radiation and MD resonances. Owing to the free-carrier injection, this leads to a size-dependent transient modulation in the refractive indices of the particle material and, therefore, to a spectral shift of the MD resonances by a different amount depending on the particle size. As a result, the light scattering diagram formed by the supercell changes under optical pumping. For the probe beam incident on the metasurface, the effect manifests itself in the redistribution of light energy between the diffraction orders (i.e., in the intensity change of the selected diffraction order, see Figure 1b). The typical time of intensity modulation is determined by free-carrier dynamics and is usually several picoseconds for structured materials based on widely used semiconductors and an order of magnitude larger for bulk materials.[37]

https://doi.org/10.1021/acsphotonics.5c01744
ACS Photonics 2025, 12, 6254−6261

Samples. In our study, we used a transparent metasurface made of GaAs. The sample was made using the sequence of standard nanofabrication methods such as molecular beam epitaxy (MBE), electron beam lithography (EBL), and reactive ion etching (RIE).[47] First, using MBE, a thin crystalline GaAs film (200 nm) was grown on the GaAs substrate with an intermediate sacrificial AlGaAs layer. By the EBL method, we created a negative resistive mask repeating the shape of initial numerical design on top of the film and etched through it using the RIE technique. Then, the structure was passivated by atomic layer deposition (ALD) of the Al_2O_3 film and transferred to the SiO_2 substrate using transparent epoxy glue, followed by removing the backside GaAs wafer by polishing and wet etching methods. The detailed fabrication procedure is described in Supporting Information, Section SM1.

The scanning electron microscopy image of the metasurface sample is shown in Figure 1c. Each supercell contains three GaAs particles, which are 200 nm-height truncated square pyramids embedded in an Al_2O_3 cladding and covered by a 50 nm-thick AlGaO layer, as schematized in Figure 1d. The side lengths of the particles are 95 ± 5, 120 ± 5, and 140 ± 5 nm for the upper edge and 125 ± 5, 135 ± 5, and 155 ± 5 nm for the base edge (see Supporting Information, Section SM2 for details). In the *X*-direction, the period of the supercell stack is 3 μm. This allows the metasurface to act as a diffraction grating in the wavelength range from 700 to 1000 nm. Along the *Y*-axis, the period is 500 nm. The distance between the centers of the supercell's particles is 500 nm. The overall size of the metasurface is 100 × 100 μm^2. Each particle of the supercell supports an MD resonance in the vicinity of a wavelength of 835 nm (Supporting Information, Section SM3).

The MD resonance provides a stronger electromagnetic field confinement within the volume of the nanoparticles compared to the electric dipole resonance. On the other hand, the wavelength of 835 nm corresponds to the GaAs band gap, ensuring efficient absorption of light. Therefore, using MD resonances at the proposed wavelength allows for a significant reduction in the pump fluence while achieving noticeable changes in the optical constants. Due to the high absorption, the number of particles in the supercell was reduced to three to increase metasurface transmission, while maintaining a period sufficient to achieve clear spatial separation of diffraction orders.

Experimental Technique. We performed the experiment using back focal plane imaging combined with a frequency degenerated pump−probe technique based on a Ti:Sa femtosecond laser (Figure 2a). The experimental setup is detailed in Supporting Information, Section SM4. Pump and probe laser pulses with a duration of 150 fs and X- and Y-polarizations (aligned parallel and perpendicular to the larger supercell period) were focused at the GaAs metasurface (Figure 2b) to a 50-μm wide spot at angles of 3 and 0°, respectively. Typical energy in the pump pulse was from 0.1 to 0.2 nJ, corresponding to a fluence of a few $\mu J/cm^2$, while the energy of the probe pulse was 10 times lower. The transmitted radiation was collected using an objective lens with NA = 0.9, the images in the front and back focal planes (BFP) of which were simultaneously analyzed. The typical BFP image is shown in Figure 2c. Each point of the image represents the intensity of light scattered by the metasurface at a certain angle. The light intensities at the diffraction maxima are determined by the scattering indicatrix of the single supercell along its long

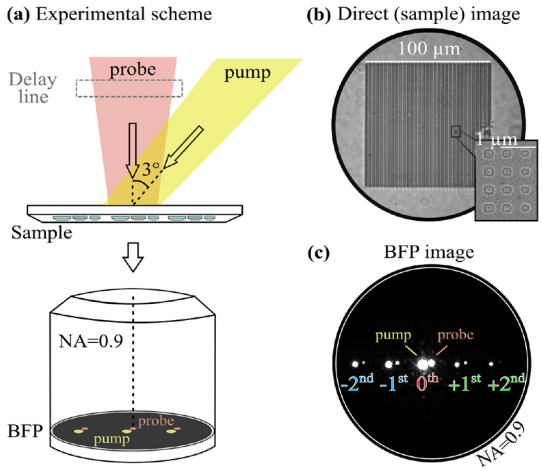

Figure 2. (a) Schematic of the pump−probe experiment combined with back focal plane imaging microscopy. (b) Front focal plane image of the metasurface used to align the probe and pump beams. Inset is a SEM image of supercells. (c) Back focal plane image showing light intensity of diffraction orders with m = 0, ±1, and ±2. NA—numerical aperture; BFP—back focal plane.

side. We have observed several pairs of spots, the positions of which are associated with different diffraction orders. The spots in each pair correspond to the pump and probe beams, and the distance between them is determined by the difference between their angles of incidence on the sample. Using a pinhole placed in the intermediate BFP image, we can select any diffracted probe beam and carry out separate spectroscopy and pump−probe measurements.

Spectroscopy. The transmittance spectra of the metasurface measured for diffraction orders m = 0, ±1 of the probe beam in the absence of the pump beam are shown in Figure 3a. Transmittance T is defined as the ratio of the intensity of the diffracted light in the corresponding direction to the intensity of the incident light. Three transmission dips are observed in the spectrum of the zeroth-order diffraction beam at wavelengths of 770, 835, and 980 nm. Corresponding electric and magnetic field distributions for the supercell are shown in Figure S6 in Supporting Information, Section SM5. The right spectral feature at 980 nm is attributed to diffraction on a periodic array without a significant contribution from the geometrical resonances of the nanoparticles. The left dip at 770 nm has a complex nature and is attributed to the interplay between MD resonances of the nanoparticles, grating resonance of the structure, and Fabry−Perot type mode excited in the Al_2O_3 passivation layer. The central dip at 835 nm corresponds to the MD resonance excitation in the GaAs nanoantennas, as confirmed by numerical modeling. Below, we focus on this spectral feature and consider it in more details.

For the transmission dip at 835 nm, an increase in the intensity of the ±1st diffraction orders reveals the directional light scattering by the supercells, which leads to the partial redistribution of light between the diffraction orders. The maximum value of 8% of the incident intensity is observed for the selected −1st diffraction order, while the intensity for the +1st diffraction order is only 3%. The zeroth-order transmission minimum of 48% is observed at the same wavelength. The results are supported by the calculations (Figure 3b), demonstrating qualitative agreement with the experiment. Experimental BFP images obtained in the spectral interval from 700 to 910 nm and normalized to the maximum intensity

https://doi.org/10.1021/acsphotonics.5c01744
ACS Photonics 2025, 12, 6254−6261

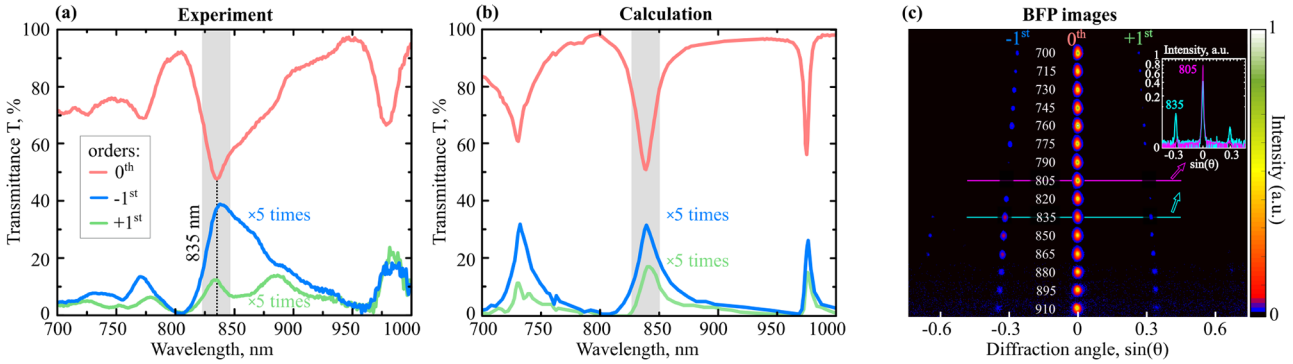

Figure 3. Experimental (a) and calculated (b) transmission spectra of three diffraction orders of the metasurface for the probe beam (the red curve is 0th order, the blue curve is −1st order, and the green curve is +1st order). (c) Series of BFP images taken at different wavelengths with a fixed average probe power of 1 mW. Inset shows the intensities of the diffraction orders at wavelengths of 835 and 805 nm.

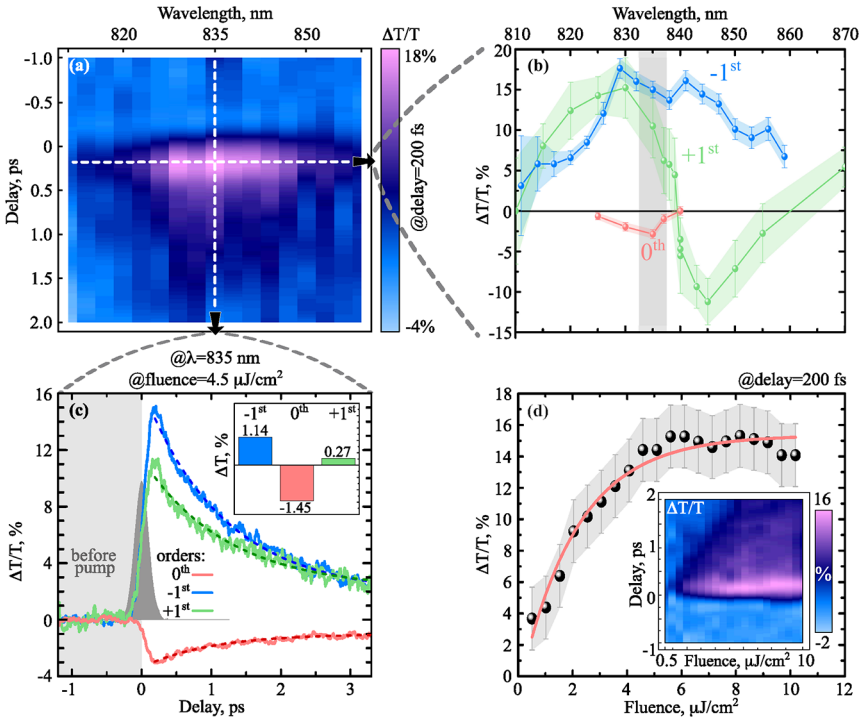

Figure 4. (a) Experimental 3D map for relative photoinduced changes $\Delta T/T$ in transmittance for the −1st diffraction order as a function of the wavelength and the pump−probe delay. (b) Slice of the 3D map at a fixed delay of 200 fs and a fluence of 4.5 μJ/cm^2: $\Delta T/T$ values for the ±1st and 0th diffraction orders as a function of the wavelength. (c) Slice of the 3D map at a fixed wavelength of 835 nm and a fluence of 4.5 μJ/cm^2: $\Delta T/T$ values for the ±1st and 0th diffraction orders (solid curves) as a function of the pump−probe delay. The dashed curves are the result of a single-exponential approximation. The pump femtosecond pulse is depicted by a gray shaded area. The inset shows an absolute change ΔT in transmittance of the diffraction orders at a delay of 200 fs. (d) Experimental intensity modulation at a fixed delay of 200 fs and a resonance wavelength of 835 nm: $\Delta T/T$ of the −1st diffraction order (dots) as a function of the pump fluence. The red curve is the result of an exponential approximation. The inset shows the experimental 3D map of $\Delta T/T$ for the −1st diffraction order as functions of the pump fluence and the pump−probe delay.

in each image are shown in Figure 3c. In the inset, two profiles at 805 and 835 nm indicate the minimum and maximum levels of the −1st order, respectively.

Pump−Probe Measurements. The relative photoinduced change $\Delta T/T$ in the intensity of the −1st diffraction order is shown in Figure 4a as a function of the time delay and the pulse wavelength for a pump fluence of 4.5 μJ/cm^2. The maximum modulation amplitude strongly depends on the wavelength and in the wavelength range from 830 to 840 nm reaches 16%. The spectral dependence of the peak intensity modulation of diffraction orders at a 200 fs delay is shown in Figure 4b. The enhancement of the −1st diffraction order intensity is observed in the entire studied spectral range with the maximum in the vicinity of an MD resonance wavelength of 835 nm. For the zeroth order, the intensity suppression is found only at the resonance wavelength, while outside the resonance, the optical modulation is not detected. In turn, the relative modulation of the +1st order is comparable in magnitude to the modulation of the −1st order, but has a nonmonotonic spectral dependence crossing zero and reaching the negative value of −12% in the vicinity of a wavelength of 845 nm.

Figure 4c depicts ultrafast dynamics of $\Delta T/T$ at a resonance wavelength of 835 nm for ±1st and zeroth diffraction orders.

https://doi.org/10.1021/acsphotonics.5c01744
ACS Photonics 2025, 12, 6254−6261

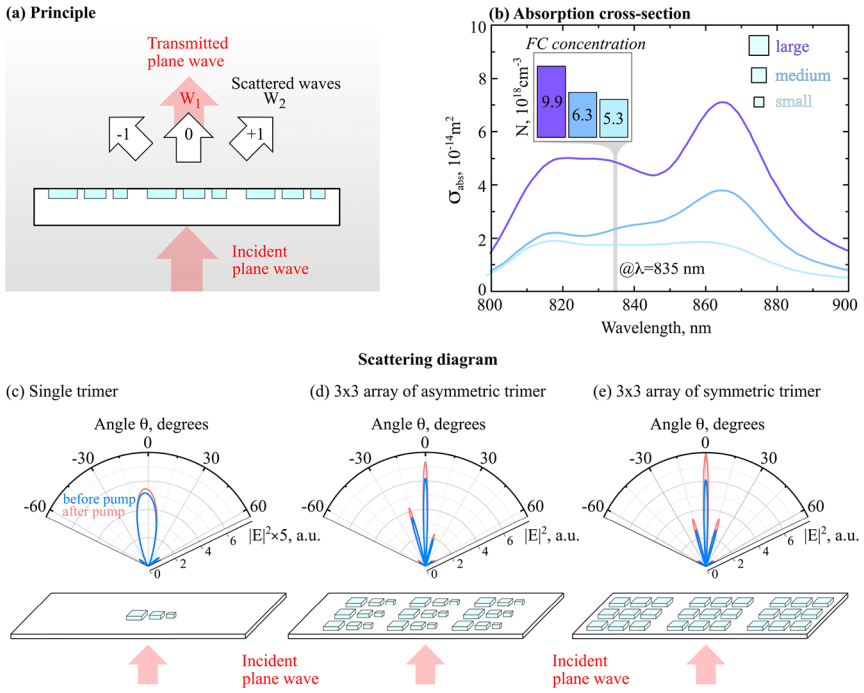

Figure 5. Numerical simulations: (a) Scheme of the sample and propagating waves. (b) Absorption cross sections for various GaAs particles forming the single supercell; the inset shows the density of free carriers generated inside each particle upon absorption of pump radiation at a wavelength of 835 nm. (c–e) Scattering diagrams for the single supercell (multiplied by 5) (c) and 3 by 3 arrays of asymmetric (d) and symmetric (e) supercells at a wavelength of 835 nm.

For all three beams, maximum modulation is obtained at approximately 200 fs after the pump pulse, and then 1.2 ps relaxation is observed for ±1st, and 1.0 ps relaxation is observed for zeroth, which are typical for the GaAs subwavelength nanoparticles.[37] The relative intensity variation $\Delta T/T$ of the −1st diffraction order is positive and reaches 15%, while the modulation of the zeroth diffraction order is negative with a maximum amplitude of about 3%. The effect of the energy redistribution is clearly seen in the inset of Figure 4c, showing an absolute change in ΔT in the transmittance of the orders at a 200 fs delay. The total increase in the intensities of ±1st orders is almost equal to the decrease in the intensity of the zeroth order.

Finally, the maximum intensity modulation of the −1st diffraction order versus the pump fluence is measured for the resonance wavelength of 835 nm (Figure 4d). Saturation is observed starting from a fluence of 5 μJ/cm^2, which limits the modulation amplitude $\Delta T/T$ to 15%. Nevertheless, we obtain sufficient intensity changes of several percents in diffraction orders, even with very weak fluences as low as 1 μJ/cm^2, that is a few orders of magnitude less than in the case of ultrafast modulation of the reflection coefficient using semiconductor metasurfaces.[37,52] Detailed comparisons between the achieved results and other works are provided in Supporting Information, Section SM6. This result demonstrates flexible control of the light intensity by the metasurface through subpicosecond modification of the scattering diagram.

Simulations. To support the experimental results, we performed numerical simulations using the FDTD method. The sample consists of parallelepipedal 200 nm-height GaAs particles with side lengths of 130, 140, and 160 nm and is illuminated through the substrate by a plane wave with a wavelength of 835 nm (Figure 5a). The nanoparticles are covered by a 50 nm-thick AlGaO layer (Figure S3c). First, we calculated the electric field distribution inside the nanoparticles at different wavelengths corresponding to the positions of the dips in the transmission spectrum of the metasurface. At a wavelength of 835 nm, the field distribution has a vortex-like shape typical of MD resonance (Figure S4). The field concentrates more strongly inside the large particle. A decrease in field localization with decreasing particle size is a result of the growing detuning between the light wavelength and the MD resonance.

We then calculated the absorption cross-section spectra of the nanoantennas in the supercell (Figure 5b). The absorption cross-section increases with growing particle size within the spectral region under study, which correlates with increasing field localization inside larger particles. This results in different concentrations of free carriers generated inside the nanoantennas under pumping, which are calculated to be $N_{small} \simeq 5.3 \times 10^{18}$cm^{-3}, $N_{medium} \simeq 6.3 \times 10^{18}$cm^{-3}, and $N_{large} \simeq 9.9 \times 10^{18}$cm^{-3} for the small, medium, and large particles, respectively, at a fluence of 4.5 μJ/cm^2 and a wavelength of 835 nm (see Supporting Information, Section SM8 for details). Knowing the concentrations, we can determine the changes in the refractive index and absorption of the nanoparticle material under pumping due to the free-carrier effect[46] (see Supporting Information, Section SM7 for details). Finally, the scattering diagrams of the single supercell and the metasurface can be calculated in the presence and absence of pump radiation.

Figure 5c shows scattering diagrams calculated for the single supercell before (blue curve) and after (red curve) laser pumping, generating free carriers with the concentrations obtained above. Initially, the main scattering lobe deviates from the normal due to the different particle sizes in the supercell. After pumping, the lobe slightly tilts to the right, and the overall intensity of the scattered light increases. We attribute the increase in intensity mainly to a decrease in

https://doi.org/10.1021/acsphotonics.5c01744
ACS Photonics 2025, 12, 6254−6261

absorption due to the saturation effect, and the lobe tilt to different changes in the refractive index of the particles. Figure 5d shows scattering diagrams calculated for the 3 × 3 array of the same supercells arranged as in the metasurface under study. Scattering maxima are seen at angles of 0 and 16−21°, corresponding to the zeroth and ±1st diffraction orders at a wavelength of 835 nm, respectively. Asymmetry in the scattering pattern of the single supercell leads to an enhancement of light scattering in one diffraction order and to a suppression of light scattering in another diffraction order. The injection of free carriers results in an increase in the intensity of light scattered in all diffraction orders. The relative change in intensity of the −1 diffraction order is approximately 17%, which is very close to the experimental value. The scattering diagram for a 3 × 3 array of supercells formed only by the large particles is shown in Figure 5e for comparison and is symmetrical.

Discussion. The intensity of the scattered light in both ±1st and zeroth diffraction orders increases under pumping. However, in the experiment, only −1st and +1st diffraction orders show intensity increases, while the zeroth order demonstrates opposite behavior. This effect can be explained by combining several phenomena in the following way. Since the particles occupy only 8−10% of the metasurface, the amount of light transmitted through the metasurface is considerable. The total observed signal is the result of the interference between transmitted W_1 and scattered W_2 waves (Figure 5a). For the zeroth diffraction order, the numerical model gives a ratio of the intensities of scattered and transmitted light of $I_2/I_1 \sim 6\%$. The total intensity in this order is

$$I = I_1 + I_2 + 2\sqrt{I_1 \times I_2}\cos(\varphi_1 - \varphi_2)$$

where φ_1 and φ_2 are the phases of the transmitted and scattered waves, respectively. Calculations show that the phase difference $\varphi_1 - \varphi_2$ is close to π (see Supporting Information, Section SM9). Thus, W_1 and W_2 interfere destructively in the direction of the zeroth diffraction order. As the intensity of the scattered light increases during laser pumping, the $\Delta T/T$ value for the zeroth order is negative and is estimated by this numerical model to be −4%, which is close to the experimentally obtained value. For ±1st diffraction orders, the total light intensity increases because only the scattered light waves propagate at the angles corresponding to these diffraction orders. The obtained values of transmittance modulation are in good comparison with those calculated using direct FDTD simulations (see Supporting Information, Section SM10). Changing the light wavelength leads to the modification of both the scattering diagram and phase relations between the transmitted and scattered waves.

Furthermore, we investigated polarization control within the asymmetric metasurface structure. We demonstrated that the distinct responses of polarizations parallel and perpendicular to the supercell axis lead to different resonance excitations and transmission behaviors for radiation initially polarized along the diagonal or circular states. The metasurface imposes phase delays that differentially affect the polarization components, resulting in nonuniform variations of the azimuth and ellipticity across the various diffraction orders. Specifically, one diffraction order exhibits predominantly azimuthal polarization changes under pumping, while another shows primarily ellipticity modulation. In contrast, the zeroth diffraction order experiences minimal polarization alteration, consistent with our earlier observation that most of the transmitted radiation in this order remains essentially unchanged. A detailed analysis of polarization control in the diffraction orders is provided in Supporting Information, Section SM11.

CONCLUSIONS

Subpicosecond all-optical control of light diffraction by novel-designed nonsymmetrical semiconductor metasurfaces composed of Mie-resonant GaAs nanoparticle clusters is experimentally observed. The observed effect corresponds to the femtosecond photoinduced generation of free carriers in the GaAs nanoparticles, which leads to the change of the IR scattering indicatrix and consequent reshaping of the metasurface diffraction efficiency. This mechanism allows us to achieve the optically induced modulation of the intensity of the transmitted light in the $m = 0, \pm 1$ diffraction orders, reaching 16% at a pump fluence as low as 4.5 $\mu J/cm^2$ with a characteristic switching time of 200 fs and a relaxation time of 1.2 ps. Results show an order of magnitude reduction in the required switching energy compared to previous studies that paves the way for new ultrafast low-power devices for efficient spatial light control.

ASSOCIATED CONTENT

Data Availability Statement

Correspondence and requests for materials should be addressed to Andrey A. Fedyanin.

Supporting Information

The Supporting Information is available free of charge at https://pubs.acs.org/doi/10.1021/acsphotonics.5c01744.

Detailed description of sample fabrication and determination of geometric parameters, femtosecond optical pump−probe setup scheme with time-resolved Fourier plane imaging microscopy, absorbance and transmittance calculations, and free-carriers calculations (PDF)

AUTHOR INFORMATION

Corresponding Author

Andrey A. Fedyanin − *Faculty of Physics, Lomonosov Moscow State University, Moscow 119991, Russia;* orcid.org/0000-0003-4708-6895; Email: fedyanin@nanolab.phys.msu.ru

Authors

Dmitry N. Gulkin − *Faculty of Physics, Lomonosov Moscow State University, Moscow 119991, Russia;* orcid.org/0000-0002-7694-7204

Alexander S. Shorokhov − *Faculty of Physics, Lomonosov Moscow State University, Moscow 119991, Russia;* orcid.org/0000-0001-8415-2623

Viacheslav S. Snigirev − *Faculty of Physics, Lomonosov Moscow State University, Moscow 119991, Russia*

Sarkis A. Dagesyan − *Faculty of Physics, Lomonosov Moscow State University, Moscow 119991, Russia*

Evgeny A. Kelm − *Faculty of Physics, Lomonosov Moscow State University, Moscow 119991, Russia*

Vladimir O. Bessonov − *Faculty of Physics, Lomonosov Moscow State University, Moscow 119991, Russia;* orcid.org/0000-0002-2165-1924

Complete contact information is available at: https://pubs.acs.org/10.1021/acsphotonics.5c01744

Author Contributions

D.N.G. and V.O.B. developed and assembled the pump−probe setup. A.S.S. suggested initial idea. D.N.G. conducted the optical experiments. A.S.S. and V.S.S. performed the numerical simulations. A.S.S. and E.A.K. developed the sample fabrication. S.A.D. and E.A.K. fabricated the samples. S.A.D. performed the SEM measurements. D.N.G. and V.O.B. prepared the first draft of the manuscript. D.N.G. prepared the figures. D.N.G., V.O.B., and A.S.S. contributed to the data analysis. A.S.S., V.O.B., and A.A.F. supervised the project and proofread the manuscript. All authors contributed to the discussion of the results and preparation of the manuscript.

Funding

Authors are grateful for financial supports from the Russian Science Foundation (Grant No. 25-12-00355).

Notes

The authors declare no competing financial interest.

■ ACKNOWLEDGMENTS

The authors acknowledge Sergey V. Ivanov for help with fabrication of heterostructures, Ivan S. Vasil'evskii for help with ALD, Vladislav A. Sitnianskii for calculation support, and Maksim V. Ryabko and Stanislav V. Polonsky for fruitful discussion.

■ REFERENCES

(1) Zheludev, N. I.; Kivshar, Y. S. From metamaterials to metadevices. *Nature Mat* **2012**, *11*, 917.
(2) Chai, Z.; Hu, X.; Wang, F.; Niu, X.; Xie, J.; Gong, Q. Ultrafast all-optical switching. *Adv. Opt. Mater.* **2017**, *5*, No. 1600665.
(3) Wang, H.; Hu, Z.; Deng, J.; Zhang, X.; Chen, J.; Li, K.; Li, G. All-optical ultrafast polarization switching with nonlinear plasmonic metasurfaces. *Sci. Adv.* **2024**, *10*, No. eadk3882.
(4) Sun, Z.; Martinez, A.; Wang, F. Optical modulators with 2D layered materials. *Nat. Photonics* **2016**, *10*, 227−238.
(5) Masharin, M. A.; Oskolkova, T.; Isik, F.; Volkan Demir, H.; Samusev, A. K.; Makarov, S. V. Giant Ultrafast All-Optical Modulation Based on Exceptional Points in Exciton−Polariton Perovskite Metasurfaces. *ACS Nano* **2024**, *18*, 3447−3455.
(6) Shaltout, A. M.; Shalaev, V. M.; Brongersma, M. L. Spatiotemporal light control with active metasurfaces. *Science* **2019**, *364*, No. eaat3100.
(7) Chen, X.; Xue, Y.; Sun, Y.; Shen, J.; Song, S.; Zhu, M.; Song, Z.; Cheng, Z.; Zhou, P. Neuromorphic Photonic Memory Devices Using Ultrafast Non-Volatile Phase-Change Materials. *Adv. Mater.* **2023**, *35*, No. 2203909.
(8) Frizyuk, K.; Melik-Gaykazyan, E.; Choi, J.-H.; Petrov, M. I.; Park, H.-G.; Kivshar, Y. Nonlinear circular dichroism in Mie-resonant nanoparticle dimers. *Nano Lett.* **2021**, *21*, 4381−4387.
(9) Rutckaia, V.; Heyroth, F.; Novikov, A.; Shaleev, M.; Petrov, M.; Schilling, J. Quantum dot emission driven by Mie resonances in silicon nanostructures. *Nano Lett.* **2017**, *17*, 6886−6892.
(10) Kroychuk, M. K.; Shorokhov, A. S.; Yagudin, D. F.; Rakhlin, M. V.; Klimko, G. V.; Toropov, A. A.; Shubina, T. V.; Fedyanin, A. A. Quantum Dot Photoluminescence Enhancement in GaAs Nanopillar Oligomers Driven by Collective Magnetic Modes. *Nanomaterials* **2023**, *13*, 507.
(11) Gulkin, D. N.; Popkova, A. A.; Afinogenov, B. I.; Shilkin, D. A.; Kuršelis, K.; Chichkov, B. N.; Bessonov, V. O.; Fedyanin, A. A. Mie-driven directional nanocoupler for Bloch surface wave photonic platform. *Nanophotonics* **2021**, *10*, 2939−2947.
(12) Kivshar, Y.; Miroshnichenko, A. Meta-optics with Mie resonances. *Optics and Photonics News* **2017**, *28*, 24−31.
(13) Staude, I.; Miroshnichenko, A. E.; Decker, M.; Fofang, N. T.; Liu, S.; Gonzales, E.; Dominguez, J.; Luk, T. S.; Neshev, D. N.; Brener, I.; Kivshar, Y. Tailoring directional scattering through magnetic and electric resonances in subwavelength silicon nanodisks. *ACS Nano* **2013**, *7*, 7824−7832.
(14) Shibanuma, T.; Matsui, T.; Roschuk, T.; Wojcik, J.; Mascher, P.; Albella, P.; Maier, S. A. Experimental demonstration of tunable directional scattering of visible light from all-dielectric asymmetric dimers. *ACS Photonics* **2017**, *4*, 489−494.
(15) Obydennov, D. V.; Shilkin, D. A.; Gulkin, D. N.; Lyubin, E. V.; Zhigunov, D. M.; Bessonov, V. O.; Fedyanin, A. A. Asymmetric Silicon Dimers Made by Single-Shot Laser-Induced Transfer Demultiplex Light of Different Wavelengths. *Adv. Opt. Mater.* **2024**, *12*, No. 2302276.
(16) Kuznetsov, A. I.; Miroshnichenko, A. E.; Brongersma, M. L.; Kivshar, Y. S.; Luk'yanchuk, B. Optically resonant dielectric nanostructures. *Science* **2016**, *354*, No. aag2472.
(17) Decker, M.; Staude, I. Resonant dielectric nanostructures: a low-loss platform for functional nanophotonics. *J. Opt.* **2016**, *18*, 103001.
(18) Kuznetsov, A. I.; et al. Roadmap for Optical Metasurfaces. *ACS Photonics* **2024**, *11*, 816−865.
(19) Liu, H.; Yang, H.; Li, Y.; Song, B.; Wang, Y.; Liu, Z.; Peng, L.; Lim, H.; Yoon, J.; Wu, W. Switchable All-Dielectric Metasurfaces for Full-Color Reflective Display. *Adv. Opt. Mater.* **2019**, *7*, No. 1801639.
(20) Shalaev, M. I.; Sun, J.; Tsukernik, A.; Pandey, A.; Nikolskiy, K.; Litchinitser, N. M. High-efficiency all-dielectric metasurfaces for ultracompact beam manipulation in transmission mode. *Nano Lett.* **2015**, *15*, 6261−6266.
(21) Yu, Y. F.; Zhu, A. Y.; Paniagua-Domínguez, R.; Fu, Y. H.; Luk'yanchuk, B.; Kuznetsov, A., I High-transmission dielectric metasurface with 2π phase control at visible wavelengths. *Laser Photonics Rev.* **2015**, *9*, 412−418.
(22) Wang, L.; Kruk, S.; Koshelev, K.; Kravchenko, I.; Luther-Davies, B.; Kivshar, Y. Nonlinear wavefront control with all-dielectric metasurfaces. *Nano Lett.* **2018**, *18*, 3978−3984.
(23) Ding, F.; Pors, A.; Bozhevolnyi, S. I. Gradient metasurfaces: a review of fundamentals and applications. *Rep. Prog. Phys.* **2018**, *81*, No. 026401.
(24) Shi, Z.; Khorasaninejad, M.; Huang, Y.-W.; Roques-Carmes, C.; Zhu, A. Y.; Chen, W. T.; Sanjeev, V.; Ding, Z.-W.; Tamagnone, M.; Chaudhary, K.; Devlin, R. C.; Qiu, C.-W.; Capasso, F. Single-layer metasurface with controllable multiwavelength functions. *Nano Lett.* **2018**, *18*, 2420−2427.
(25) Sun, X.; Qu, Z.; Yuan, J.; Wang, Q. Reconfigurable broadband polarisation conversion metasurface based on VO2. *Phot. Nano. Fundam. Appl.* **2022**, *50*, No. 101012.
(26) Gigli, C.; Li, Q.; Chavel, P.; Leo, G.; Brongersma, M. L.; Lalanne, P. Fundamental Limitations of Huygens' Metasurfaces for Optical Beam Shaping. *Laser Photonics Rev.* **2021**, *15*, No. 2000448.
(27) Faraji-Dana, M.; Arbabi, E.; Arbabi, A.; Kamali, S. M.; Kwon, H.; Faraon, A. Compact folded metasurface spectrometer. *Nat. Commun.* **2018**, *9*, 4196.
(28) Cai, G.; Li, Y.; Zhang, Y.; Jiang, X.; Chen, Y.; Qu, G.; Zhang, X.; Xiao, S.; Han, J.; Yu, S.; Kivshar, Y.; Song, Q. Compact angle-resolved metasurface spectrometer. *Nat. Mater.* **2024**, *23*, 71−78.
(29) Choi, C.; Lee, S.-Y.; Mun, S.-E.; Lee, G.-Y.; Sung, J.; Yun, H.; Yang, J.-H.; Kim, H.-O.; Hwang, C.-Y.; Lee, B. Metasurface with nanostructured $Ge_2Sb_2Te_5$ as a platform for broadband-operating wavefront switch. *Adv. Opt. Mater.* **2019**, *7*, No. 1900171.
(30) Rao, R.; Shi, Y.; Wang, Z.; Wan, S.; Li, Z. On-Chip Cascaded Metasurfaces for Visible Wavelength Division Multiplexing and Color-Routing Meta-Display. *Nano Lett.* **2025**, *25*, 2452−2458.
(31) Chu, C. H.; Tseng, M. L.; Chen, J.; Wu, P. C.; Chen, Y.-H.; Wang, H.-C.; Chen, T.-Y.; Hsieh, W. T.; Wu, H. J.; Sun, G.; Tsai, D. P. Active dielectric metasurface based on phase-change medium. *Laser Photonics Rev.* **2016**, *10*, 986−994.
(32) Komar, A.; Paniagua-Dominguez, R.; Miroshnichenko, A.; Yu, Y. F.; Kivshar, Y. S.; Kuznetsov, A. I.; Neshev, D. Dynamic beam switching by liquid crystal tunable dielectric metasurfaces. *ACS Photonics* **2018**, *5*, 1742−1748.

https://doi.org/10.1021/acsphotonics.5c01744
ACS Photonics 2025, 12, 6254−6261

(33) Rocco, D.; Gandolfi, M.; Tognazzi, A.; Pashina, O.; Zograf, G.; Frizyuk, K.; Gigli, C.; Leo, G.; Makarov, S.; Petrov, M.; De Angelis, C. Opto-thermally controlled beam steering in nonlinear all-dielectric metastructures. *Opt. Express* **2021**, *29*, 37128−37139.
(34) Sivan, Y.; Spector, M. Ultrafast dynamics of optically induced heat gratings in metals. *ACS Photonics* **2020**, *7*, 1271−1279.
(35) Wang, Y.; Landreman, P.; Schoen, D.; Okabe, K.; Marshall, A.; Celano, U.; Wong, H. S. P.; Park, J.; Brongersma, M. L. Electrical tuning of phase-change antennas and metasurfaces. *Nat. Nanotechnol.* **2021**, *16*, 667−672.
(36) Ding, F.; Meng, C.; Bozhevolnyi, S. I. *Electrically tunable optical metasurfaces. Photonics Insights* **2024**, *3*, R07−R07.
(37) Shcherbakov, M. R.; Liu, S.; Zubyuk, V. V.; Vaskin, A.; Vabishchevich, P. P.; Keeler, G.; Pertsch, T.; Dolgova, T. V.; Staude, I.; Brener, I.; Fedyanin, A. A. Ultrafast all-optical tuning of direct-gap semiconductor metasurfaces. *Nat. Commun.* **2017**, *8*, 17.
(38) Baranov, D. G.; Makarov, S. V.; Krasnok, A. E.; Belov, P. A.; Alù, A. Tuning of near-and far-field properties of all-dielectric dimer nanoantennas via ultrafast electron-hole plasma photoexcitation. *Laser Photonics Rev.* **2016**, *10*, 1009−1015.
(39) Crotti, G.; Schirato, A.; Pashina, O.; Sergaeva, O.; Petrov, M.; De Angelis, C.; Della Valle, G. Ultrafast switching of a metasurface quasi-bound state in the continuum via transient optical symmetry breaking. *Light: Sci. Appl.* **2025**, *14*, 240.
(40) Schirato, A.; Maiuri, M.; Toma, A.; Fugattini, S.; Proietti Zaccaria, R.; Laporta, P.; Nordlander, P.; Cerullo, G.; Alabastri, A.; Della Valle, G. Transient optical symmetry breaking for ultrafast broadband dichroism in plasmonic metasurfaces. *Nat. Photonics* **2020**, *14*, 723−727.
(41) Cui, T.; Bai, B.; Sun, H.-B. Tunable metasurfaces based on active materials. *Adv. Funct. Mater.* **2019**, *29*, No. 1806692.
(42) Abdelraouf, O. A.; Wang, Z.; Liu, H.; Dong, Z.; Wang, Q.; Ye, M.; Wang, X. R.; Wang, Q. J.; Liu, H. Recent advances in tunable metasurfaces: materials, design, and applications. *ACS Nano* **2022**, *16*, 13339−13369.
(43) Shcherbakov, M. R.; Vabishchevich, P. P.; Shorokhov, A. S.; Chong, K. E.; Choi, D.-Y.; Staude, I.; Miroshnichenko, A. E.; Neshev, D. N.; Fedyanin, A. A.; Kivshar, Y. S. Ultrafast all-optical switching with magnetic resonances in nonlinear dielectric nanostructures. *Nano Lett.* **2015**, *15*, 6985−6990.
(44) Galiffi, E.; Tirole, R.; Yin, S.; Li, H.; Vezzoli, S.; Huidobro, P. A.; Silveirinha, M. G.; Sapienza, R.; Alù, A.; Pendry, J. B. Photonics of time-varying media. *Adv. Photonics* **2022**, *4*, No. 014002.
(45) Genevet, P.; Capasso, F.; Aieta, F.; Khorasaninejad, M.; Devlin, R. Recent advances in planar optics: from plasmonic to dielectric metasurfaces. *Optica* **2017**, *4*, 139−152.
(46) Bennett, B. R.; Soref, R. A.; Del Alamo, J. A. Carrier-induced change in refractive index of InP, GaAs and InGaAsP. *IEEE J. Quantum Electron.* **1990**, *26*, 113−122.
(47) Liu, S.; Keeler, G. A.; Reno, J. L.; Sinclair, M. B.; Brener, I. III−V semiconductor nanoresonators —A new strategy for passive, active, and nonlinear all-dielectric metamaterials. *Adv. Opt. Mater.* **2016**, *4*, 1457−1462.
(48) Zubyuk, V. V.; Vabishchevich, P. P.; Shcherbakov, M. R.; Shorokhov, A. S.; Fedotova, A. N.; Liu, S.; Keeler, G.; Dolgova, T. V.; Staude, I.; Brener, I.; Fedyanin, A. A. Low-Power Absorption Saturation in Semiconductor Metasurfaces. *ACS Photonics* **2019**, *6*, 2797−2806.
(49) Makarov, S.; Kudryashov, S.; Mukhin, I.; Mozharov, A.; Milichko, V.; Krasnok, A.; Belov, P. Tuning of magnetic optical response in a dielectric nanoparticle by ultrafast photoexcitation of dense electron−hole plasma. *Nano Lett.* **2015**, *15*, 6187−6192.
(50) Guo, P.; Schaller, R. D.; Ketterson, J. B.; Chang, R. P. Ultrafast switching of tunable infrared plasmons in indium tin oxide nanorod arrays with large absolute amplitude. *Nat. Photonics* **2016**, *10*, 267−273.
(51) Kang, T.; et al. Large-scale, power-efficient Au/VO_2 active metasurfaces for ultrafast optical modulation. *Nanophotonics* **2020**, *10*, 909−918.
(52) Vabishchevich, P. P.; Vaskin, A.; Karl, N.; Reno, J. L.; Sinclair, M. B.; Staude, I.; Brener, I. Ultrafast all-optical diffraction switching using semiconductor metasurfaces. *Appl. Phys. Lett.* **2021**, *118*, 211105.
(53) Basiri, A.; Rafique, M. Z. E.; Bai, J.; Choi, S.; Yao, Y. Ultrafast low-pump fluence all-optical modulation based on graphene-metal hybrid metasurfaces. *Light: Sci. Appl.* **2022**, *11*, 102.

https://doi.org/10.1021/acsphotonics.5c01744
ACS Photonics 2025, 12, 6254−6261